IEEE Transactions on Power Electronics, pp. 1–1, 2018

Modular Multilevel Converter Control Methods Performance Benchmark for Medium Voltage Applications

A. Christe and D. Dujic

POWER ELECTRONICS LABORATORY
ÉCOLE POLYTECHNIQUE FÉDÉRALE DE LAUSANNE

This article has been accepted for publication in a future issue of this journal, but has not been fully edited. Content may change prior to final publication. Citation information: DOI 10.1109/TPEL.2018.2865422, IEEE Transactions on Power Electronics

Modular Multilevel Converter Control Methods Performance Benchmark for Medium Voltage Applications

Alexandre Christe, *Student Member, IEEE,* Drazen Dujic, *Senior Member, IEEE*

***Abstract*—Modular multilevel converters are increasingly being considered or used for various medium voltage applications. Multiple control methods have been proposed for the control of the direct to three-phase modular multilevel converter. They differ one from another in the way the capacitor voltage ripples are handled, i.e. either neglected, estimated, reconstructed by filtering or measured. This has implications on the performance level that can be obtained. This paper provides insights on the advantages and drawbacks of each control method, in inverter and rectifier mode, with a fair and thorough assessment supported by extensive simulations, with converter ratings that are realistic for medium voltage applications. Finally, this works highlights the impact of the higher dynamics for medium voltage dc applications compared to high voltage dc ones on the choice of the control method.**

***Index Terms*—MMC, control methods.**

NOMENCLATURE

$\{a,b,c\}$	Phase
$\{p,n\}$	Positive / negative branch
m	Modulation index
ω	Grid frequency
ϕ	Load angle
$e_{\{p,n\}}$	Equivalent branch EMF voltage
V_B	Dc-side voltage
v_{CM}	Common-mode voltage
e_{circ}	Equivalent emf voltage on the dc bus side
e_L	Equivalent EMF voltage on the ac grid side
$v_{C\Sigma}$	Summed capacitor voltage in a branch
$v_{C\Sigma}^{\Sigma}$	Summed branch capacitor voltages
$v_{C\Sigma}^{\Delta}$	Differential branch capacitor voltages
I_B	Dc-side current
i_g	Grid-side current
i_{circ}	Circulating current
N_{cells}	Number of cells per branch
C_{cell}	Cell capacitance
L_{br}	Branch inductance
R_{br}	Branch resistance
C_{br}	Branch equivalent capacitance ($C_{\text{br}} = C_{\text{cell}}/N_{\text{cells}}$)

Manuscript received February 14, 2018; accepted August 7, 2018.

A. Christe was with the Power Electronics Laboratory, École Polytechnique Fédérale de Lausanne (EPFL), 1015 Lausanne, Switzerland, when this work was conducted, but is now with ABB Corporate Research Center, 722 26 Västerås, Sweden (e-mail: alexandre.christe@se.abb.com).

D. Dujic is with the Power Electronics Laboratory, École Polytechnique Fédérale de Lausanne (EPFL), 1015 Lausanne, Switzerland (e-mail: drazen.dujic@epfl.ch).

This work is part of the Swiss Competence Centers for Energy Research (SCCER) initiative which is supported by the Swiss Commission for Technology and Innovation (CTI).

Color versions of one or more of the figures in this paper are available online at http://ieeexplore.ieee.org.

Digital Object Identifier XXXXXXXX

I. INTRODUCTION

SINCE its introduction, the modular multilevel converter (MMC) [1], and especially its control and modulation methods, received a lot of attention from the researchers and the industry. It made quickly its way to market for point-to-point high voltage dc (HVdc) transmission [2], due to clear advantages over the line-commutated inverters (LCIs) and two- or three-level voltage-source converters (VSCs). The key features of an MMC are the modularity, provided by a basic cell allowing for straightforward voltage scalability, as well as the absence of a centralized direct current (dc) link capacitor, replaced by distributed capacitors in the cells.

Nowadays, more and more applications in the medium voltage (MV) range are emerging, with for example STATCOMs [3], railway supply with static frequency converters, e.g., three-phase $50\,\text{Hz}$ to single-phase $16.7\,\text{Hz}$, [4], [5], drives [6], [7], onshore power supply [8], medium voltage dc (MVdc) transmission, for power levels up to $150\,\text{MW}$ over $200\,\text{km}$ and $50\,\text{kV}_{\text{dc}}$ [9], [10], etc. At their heart is a modular structure, with multiple branches (or chain-links) [11], that offer an increased level of performance compared to monolithic designs. These were relying on parallel back-to-back converters at much lower voltages ($3-5\,\text{kV}$, e.g., 3L NPC) and complex transformer arrangements in order to cancel the low order switching harmonics, since the voltage scaling is far from being straightforward.

While MMC-based structures can perform various conversions, the scope of this paper is limited to MV dc-alternate current (ac) and ac-dc conversion with a double-star configuration. Numerous control methods have been proposed in the literature [12]–[14] and tailored for specific applications or with a specific shaping of the outer loops to achieve a desired converter behaviour. The differences stem from the way the capacitor voltage ripples are handled, i.e. either neglected, estimated, reconstructed by filtering or measured. However, the focus was never set on a comparative benchmark of their achievable performances. The objective of this paper is to fill this gap by providing an insightful and transparent comparison. Several control methods have been implemented and extensive simulations are carried out in order to provide a base for an objective discussion, which is summarized in the end.

This article has been accepted for publication in a future issue of this journal, but has not been fully edited. Content may change prior to final publication. Citation information: DOI 10.1109/TPEL.2018.2865422, IEEE Transactions on Power Electronics

The study presented in the paper is relevant for several reasons. First of all, the MV domain normally considers voltages from $1\,\mathrm{kV_{ac}}$ to $36\,\mathrm{kV_{ac}}$ (or rectified levels for dc). These are significantly lower voltage levels compared to HVdc applications. For a selected rated dc voltage, a branch requires a considerably lower number of cells in MV applications compared to the high voltage (HV) ones. Then, the power flows in the MV distribution grid are becoming increasingly complex, especially when considering all the players (distributed generation, industrial consumers, private end-users). Thus, dynamics are quite different from HV transmission grids or point-to-point HVdc links. An MMC in MV grids faces different challenges compared to situation in HVdc grids. When it comes to requirements, standards have already been edicted for marine applications [15], and a Cigré working group has been created [16].

The paper is organized as the following. Section II presents the modelling of the direct to three-phase (dc/3-ac) MMC, with the introduction of the relevant notation used throughout the paper. Section III presents a summary of the different control loops, along with their tuning. Section IV discussed the possible ways to obtain the modulation index, which prepares for the extensive benchmark simulations that follow in Section V, since it impacts the presence or absence of some control loops. The comparison is carried both in inverter mode, where the dc bus is assumed stiff, hence uncontrolled, and in rectifier mode, where the converter controls the dc link voltage. A set of performances indices are selected in order to present in a concise manner the trade-offs and benefits of each control method in the discussion in Section VI. Section VII concludes the paper.

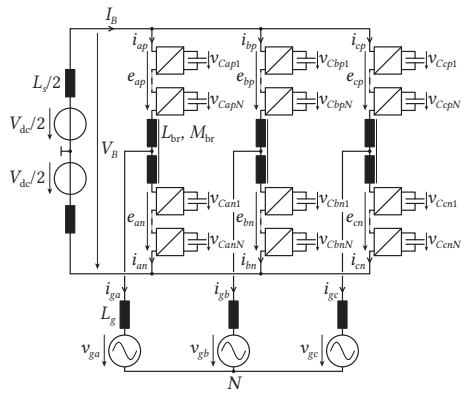

Fig. 1. Dc/3-ac MMC scheme and nomenclature.

II. Definition of the basic quantities

The dc/3-ac MMC scheme is presented in Fig. 1. Each MMC branch comprises a number of series-connected cells and a branch inductance (the non-coupled case is considered in this paper). The variables in bold denote vectors, e.g., $\mathbf{i}_p = [i_{ap}\ i_{bp}\ i_{cp}]^T$. From the loop equations, the following compact set of differential equations is obtained in (1), where $\mathbb{I}$ and $\mathbb{O}$ are the identity and null matrices, respectively, and $\mathbb{M}_{p/n} = \mathrm{diag}(\mathbf{m}_{p/n})$, with $\mathbf{m}_{p/n} = [m_{ap/n}\ m_{bp/n}\ m_{cp/n}]^T$ the vector of modulation indices. Note that matrices with a single subscript are square matrices. By introducing a new set of variables in (2) [17], a decoupled time-varying state-space model can be obtained in (3).

$$\begin{bmatrix}\mathbf{i}_{\mathrm{circ}}\\ \mathbf{i}_g\end{bmatrix} = \begin{bmatrix}\frac{1}{2}\mathbb{I}_3 & \frac{1}{2}\mathbb{I}_3\\ \mathbb{I}_3 & -\mathbb{I}_3\end{bmatrix}\begin{bmatrix}\mathbf{i}_p\\ \mathbf{i}_n\end{bmatrix} \tag{2a}$$

$$\begin{bmatrix}(L_{\mathrm{br}}+L_g)\mathbb{I}_3 & -(M_{\mathrm{br}}+L_g)\mathbb{I}_3 & \mathbb{O}_3 & \mathbb{O}_3\\ -(M_{\mathrm{br}}+L_g)\mathbb{I}_3 & (L_{\mathrm{br}}+L_g)\mathbb{I}_3 & \mathbb{O}_3 & \mathbb{O}_3\\ \mathbb{O}_3 & \mathbb{O}_3 & C_{\mathrm{br}}\mathbb{I}_3 & \mathbb{O}_3\\ \mathbb{O}_3 & \mathbb{O}_3 & \mathbb{O}_3 & C_{\mathrm{br}}\mathbb{I}_3\end{bmatrix}\frac{\mathrm{d}}{\mathrm{d}t}\begin{bmatrix}\mathbf{i}_p\\ \mathbf{i}_n\\ \mathbf{v}_{C\Sigma p}\\ \mathbf{v}_{C\Sigma n}\end{bmatrix} =$$
$$\begin{bmatrix}-(R_{\mathrm{br}}+R_g)\mathbb{I}_3 & R_g\mathbb{I}_3 & \mathbb{M}_p & \mathbb{O}_3\\ R_g\mathbb{I}_3 & -(R_{\mathrm{br}}+R_g)\mathbb{I}_3 & \mathbb{O}_3 & \mathbb{M}_n\\ \mathbb{M}_p & \mathbb{O}_3 & -\frac{1}{R_{\mathrm{esr}}}\mathbb{I}_3 & \mathbb{O}_3\\ \mathbb{O}_3 & \mathbb{M}_n & \mathbb{O}_3 & -\frac{1}{R_{\mathrm{esr}}}\mathbb{I}_3\end{bmatrix}\begin{bmatrix}\mathbf{i}_p\\ \mathbf{i}_n\\ \mathbf{v}_{C\Sigma p}\\ \mathbf{v}_{C\Sigma n}\end{bmatrix} + \begin{bmatrix}\frac{1}{2}\mathbb{I}_{3\times1} & -\mathbb{I}_3\\ \frac{1}{2}\mathbb{I}_{3\times1} & \mathbb{I}_3\\ \mathbb{O}_{3\times1} & \mathbb{O}_3\\ \mathbb{O}_{3\times1} & \mathbb{O}_3\end{bmatrix}\begin{bmatrix}V_B\\ \mathbf{v}_g + v_{\mathrm{CM}}\mathbb{I}_{3\times1}\end{bmatrix} \tag{1}$$

$$\frac{\mathrm{d}}{\mathrm{d}t}\begin{bmatrix}\mathbf{i}_{\mathrm{circ}}\\ \mathbf{i}_g\\ \mathbf{v}^{\Sigma}_{C\Sigma}\\ \mathbf{v}^{\Delta}_{C\Sigma}\end{bmatrix} = \begin{bmatrix}-\frac{R_{\mathrm{br}}}{L_{\mathrm{br}}-M\mathrm{br}}\mathbb{I}_3 & -\frac{R_{\mathrm{br}}/2+R_g}{L_{\mathrm{br}}+M_{\mathrm{br}}+2L_g}\mathbb{I}_3 & \frac{(L_{\mathrm{br}}+L_g)\mathbb{M}_p+(M_{\mathrm{br}}+L_g)\mathbb{M}_n}{2(L_{\mathrm{br}}-M_{\mathrm{br}})(L_{\mathrm{br}}+2L_g+M_{\mathrm{br}})} & -\frac{(L_{\mathrm{br}}+L_g)\mathbb{M}_p-(L_g+M_{\mathrm{br}})\mathbb{M}_n}{(L_{\mathrm{br}}-M_{\mathrm{br}})(L_{\mathrm{br}}+2L_g+M_{\mathrm{br}})}\\ -\frac{R_{\mathrm{br}}}{L_{\mathrm{br}}-M_{\mathrm{br}}}\mathbb{I}_3 & \frac{R_{\mathrm{br}}/2+R_g}{L_{\mathrm{br}}+2L_g+M_{\mathrm{br}}}\mathbb{I}_3 & \frac{(L_{\mathrm{br}}+L_g)\mathbb{M}_n+(L_g+M_{\mathrm{br}})\mathbb{M}_p}{2(L_{\mathrm{br}}-M_{\mathrm{br}})(L_{\mathrm{br}}+2L_g+M_{\mathrm{br}})} & \frac{(L_{\mathrm{br}}+L_g)\mathbb{M}_n-(L_g+M_{\mathrm{br}})\mathbb{M}_p)}{(L_{\mathrm{br}}-M_{\mathrm{br}})(L_{\mathrm{br}}+2L_g+M_{\mathrm{br}})}\\ \frac{1}{C_{\mathrm{br}}}\mathbb{M}_p & \frac{1}{2C_{\mathrm{br}}}\mathbb{M}_p & -\frac{1}{2C_{\mathrm{br}}R_{\mathrm{esr}}}\mathbb{I}_3 & \frac{1}{C_{\mathrm{br}}R_{\mathrm{esr}}}\mathbb{I}_3\\ \frac{1}{C_{\mathrm{br}}}\mathbb{M}_n & -\frac{1}{2C_{\mathrm{br}}}\mathbb{M}_n & -\frac{1}{2C_{\mathrm{br}}R_{\mathrm{esr}}}\mathbb{I}_3 & -\frac{1}{C_{\mathrm{br}}R_{\mathrm{esr}}}\mathbb{I}_3\end{bmatrix}\begin{bmatrix}\mathbf{i}_{\mathrm{circ}}\\ \mathbf{i}_g\\ \mathbf{v}^{\Sigma}_{C\Sigma}\\ \mathbf{v}^{\Delta}_{C\Sigma}\end{bmatrix}$$
$$+\begin{bmatrix}\frac{3}{4(L_{\mathrm{br}}-M_{\mathrm{br}})}\mathbb{I}_{3\times1} & -\frac{1}{2(L_{\mathrm{br}}+2L_g+M_{\mathrm{br}})}\mathbb{I}_3\\ \frac{1}{4(L_{\mathrm{br}}-M_{\mathrm{br}})}\mathbb{I}_{3\times1} & -\frac{3}{2(L_{\mathrm{br}}+2L_g+M_{\mathrm{br}})}\mathbb{I}_3\\ \mathbb{O}_{3\times1} & \mathbb{O}_3\\ \mathbb{O}_{3\times1} & \mathbb{O}_3\end{bmatrix}\begin{bmatrix}V_B\\ \mathbf{v}_g + v_{\mathrm{CM}}\mathbb{I}_{3\times1}\end{bmatrix} \tag{3}$$

This article has been accepted for publication in a future issue of this journal, but has not been fully edited. Content may change prior to final publication. Citation information: DOI 10.1109/TPEL.2018.2865422, IEEE Transactions on Power Electronics

$$\begin{bmatrix} \mathbf{v}_{C\Sigma}^{\Sigma} \\ \mathbf{v}_{C\Sigma}^{\Delta} \end{bmatrix} = \begin{bmatrix} \mathbb{I}_3 & \mathbb{I}_3 \\ -\frac{1}{2}\mathbb{I}_3 & \frac{1}{2}\mathbb{I}_3 \end{bmatrix} \begin{bmatrix} \mathbf{v}_{C\Sigma p} \\ \mathbf{v}_{C\Sigma n} \end{bmatrix} \tag{2b}$$

The presented mathematical model is generic, although an equivalent representation is used for the benchmarking, as discussed in Section V-A.

III. MMC CONTROL METHODS

The control of a dc/3-ac MMC is complex and has been extensively treated in various publications. In this work, a cascaded control architecture is adopted. The different loops can be grouped in two sets:

1) The external state variable control: ac grid currents, phase-locked loop (PLL) and dc voltage control;
2) The internal state variable control: capacitor voltages/stored energy and circulating currents.

For the former, all the knowledge from the VSC control can be applied, as from a terminal point of view an MMC behaves similarly as a two- or three-level VSC. For the latter, specific control algorithms have been developed, and these internal control loops are providing some unique attributes. Two operating modes are distinguished, depending on the nature of the source/load connected on the dc side:

1) Inverter mode (also called current source mode): the dc side voltage is assumed to be stiff (i.e. controlled by another entity), justifying the absence of dc voltage control in the MMC;
2) Rectifier mode (also called voltage source mode): the MMC controls also the dc voltage.

The overall control schemes for each operating mode are presented first (cf. Fig. 2) and the description of the control loop follows.

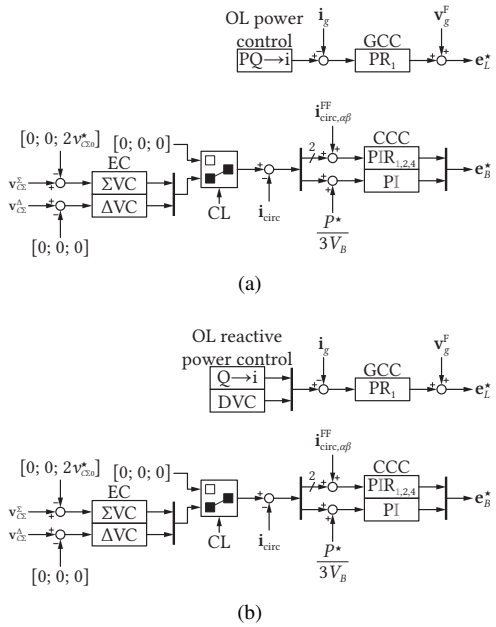

Fig. 2. Overall control schemes: (a) inverter and (b) rectifier mode. The control loops are denoted as: EC (energy control), CCC (circulating current control), OL (open-loop, with look-up tables), GCC (grid current control) and DVC (direct voltage control). CL is a control switch that depends whether the closed-loop control is activated or not. The PLL is not shown.

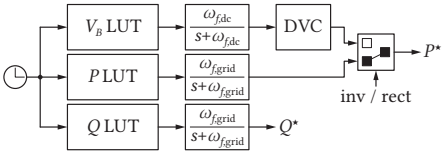

Fig. 3. Power references, with a signal selector depending on the operating mode.

A. External state variable control

1) Power references: The power references are handled in an open-loop fashion. The reference are eventually low-pass filtered in order to smoothen up the transients (cf. Fig. 3). Depending on the operating mode, either the active power reference $P^\star$ (for the inverter mode) or the dc voltage $V_B^\star$ in combination with the direct voltage control (DVC) (for the rectifier mode) is used. In any case, the reactive power component is kept for any grid ancillary / support feature.

The grid current references are determined according to [18]. From power references and grid voltages transformed into $\alpha\beta$ frame, current references for the grid current controllers are calculated.

$$\begin{bmatrix} i_{g\alpha}^\star \\ i_{g\beta}^\star \end{bmatrix} = \frac{2}{3}\frac{1}{v_{g\alpha}^2 + v_{g\beta}^2} \begin{bmatrix} v_{g\alpha} & -v_{g\beta} \\ v_{g\beta} & v_{g\alpha} \end{bmatrix} \begin{bmatrix} P^\star \\ Q^\star \end{bmatrix} \tag{4}$$

2) Grid current control (GCC): Either proportional integral (PI) in dq-frame(s) or proportional resonant (PR) [19] in $\alpha\beta$-frame are controller structures able to achieve the tracking of the ac grid current references with zero steady state error.

A PR controller in $\alpha\beta$-frame is used for the simulations presented in the next section. The controller is defined as:

$$G_{\text{PR}}(s) = K_{p,\text{gcc}} + K_{h,\text{gcc}}\frac{s\cos(\phi_h') - h\omega_1\sin(\phi_h')}{s^2 + (h\omega_1)^2} \tag{5}$$

where $\phi_h' = h\omega_1 T_d$ (with usually $T_d = 1.5T_s$ for pulse-width modulation (PWM) and computation delays). Delays are further discussed in Section V. The selection of the controller gains follows:

$$K_{p,\text{gcc}} = \alpha_{\text{gcc}}\left(L_g + L_{\text{br}}/2\right) \tag{6a}$$

$$K_{h,\text{gcc}} = 2\alpha_{h,\text{gcc}} K_{p,\text{gcc}} \tag{6b}$$

The controller bandwidth is selected such that $\alpha_{\text{gcc}} \leq 0.1\omega_s$, with ω_s the sampling frequency. The result of the controller action is summarized as:

$$\mathbf{e}_{L,\alpha\beta}^\star = G_{\text{PR}}(s)(\mathbf{i}_{L,\alpha\beta} - \mathbf{i}_{L,\alpha\beta}^\star) + \mathbf{v}_{g,\alpha\beta}^{\text{FF}} \tag{7}$$

where $\mathbf{v}_{g,\alpha\beta}^{\text{FF}}$ is the (low-pass filtered) point of common coupling (PCC) voltage measurement.

3) Phase-locked loop (PLL): The role of the PLL is to achieve a tracking of the grid angle and retrieve the grid frequency. A standard dq-PLL is used, in combination with an optional low-pass filter to get rid of undesired harmonics (i.e. ac part of the dq signals), as shown in Fig. 4. There is a trade-off between the filter cut-off frequency and the PLL dynamics. The quadrature component is normalized with the grid voltage to avoid dependency with the grid voltage magnitude. An integral part in the PLL is required in order to

This article has been accepted for publication in a future issue of this journal, but has not been fully edited. Content may change prior to final publication. Citation information: DOI 10.1109/TPEL.2018.2865422, IEEE Transactions on Power Electronics

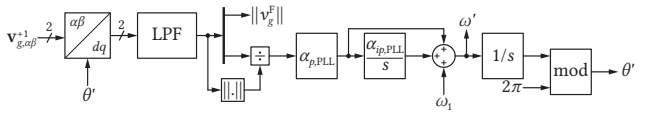

Fig. 4. PLL in dq frame, with optional low-pass filter on the dq signals ($\mathbf{v}^{\mathrm{FF}}_{g,dq}$ might be taken from there), and amplitude normalization in order to maintain the same dynamics regardless of the magnitude of the grid voltage. ω' and θ' are the estimated signals provided by the PLL. ω_1 is only there to reduce the pull-up time at the startup.

properly drive the grid angle error to zero after a frequency variation. The PLL control action is defined as:

$$\omega' = \omega_1 + \alpha_{p,\mathrm{PLL}} \left(1 + \frac{\alpha_{ip,\mathrm{PLL}}}{s}\right) \frac{v^{\mathrm{F}}_{g,q}}{||\mathbf{v}^{\mathrm{F}}_{g,dq}||} \tag{8}$$

Note that the PLL has a bandwidth at least one decade lower than the grid current control loop.

4) Dc voltage control (DVC): A dc voltage controller is only present in rectifier mode, where the converter is normally expected to regulate the dc voltage. It is preferred to control the dc energy rather than the dc voltage in order to avoid dependency with the dc voltage magnitude [20]. A low-pass filter is added on the measurement to avoid transferring undesired harmonics to the ac grid, which would lead to oscillations in the active power.

$$P^{\star} = \frac{\alpha_d C_d}{2} \left(1 + \frac{\alpha_{id}}{s}\right) \left(V_B^{\mathrm{F}2} - V_B^{\star 2}\right) \tag{9}$$

Note that the correction sign is inverted, since the direction of the currents is reversed for the sake of rectifier conventions.

B. Internal state variable control

1) Energy control (EC): The energy balancing is a control action that ensures an equal distribution of the average stored energy within the converter, i.e. that the energies among the branches are similar [21]. Two mechanisms are present: (i) the horizontal balancing and (ii) the vertical balancing. Their control implementations have been widely discussed in the literature: in [14], the horizontal balancing is performed in $dq0$ frame at twice the grid frequency, in [22], the energies are controlled in $\alpha\beta0$ coordinates with PI controllers. The balancing action shall not be visible at any converter terminal, i.e. the balancing process remains unseen from outside the converter.

a) Horizontal balancing: The horizontal balancing ensures an equal partition of the average stored energy among the three phase-legs. It modifies the sharing of the dc current among the phase-legs and interacts with the dc part of the branch voltages, which appears with the same sign for both the positive and negative branch. It leads to identical energy variation for both branches within the same phase-leg. The lowest possible value for $v^{\Sigma}_{C\Sigma 0}$ is $V_B - 2R_{\mathrm{br}}I_B/3$, since for a dc/3-ac MMC it is assumed that there is a sufficient voltage margin between the dc terminal voltage and the maximum ac peak-to-peak voltage[1]. However, in such a case, there is no margin against dc overvoltages. For control purpose and transients

[1]For unipolar cells, $m \in [0,\ 1]$.

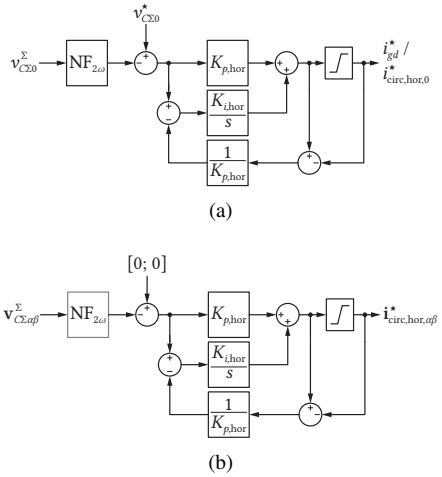

Fig. 5. Horizontal balancing in $\alpha\beta0$ frame: (a) zero sequence component, corresponding to the total energy control (with recommended notch filter especially in the case of grid faults/imbalances), and (b) $\alpha\beta$ components, corresponding to the phase-leg imbalances (with optional notch filter). In inverter mode, the zero-sequence reference is fed to the circulating current controller, while in rectifier mode it is fed to the grid current controller.

handling, there are incentives to increase $v^{\Sigma\star}_{C\Sigma 0}$. Still, its value shall not be increased too much, since efficiency constraints (higher $v^{\Sigma\star}_{C\Sigma 0}$ implies higher switching losses) and limitations from the hardware capability (maximum cell voltage) have to be accounted for. The horizontal balancing scheme is presented in Fig. 5, where the $\alpha\beta0$ frame is selected. The zero-sequence component corresponds to the total energy control, while the $\alpha\beta$ ones correspond to the energy imbalance between the phase-legs. Hence, the reference for the $\alpha\beta$ components is $[0\ 0]^T$.

b) Vertical balancing: The vertical balancing ensures an equal distribution of the stored energy between the positive and negative branch of the same phase-leg. It introduces an ac component at fundamental frequency that interacts with the fundamental ac component of the branch voltage. Power shifting between the positive and negative branch is achieved due to opposite signs of the grid voltage component in the branch voltage. In normal operation, different energy levels between the positive and negative branch are not desired. Hence the reference is set to $[0\ 0\ 0]^T$. The notch filters at fundamental frequency ensure that the controller outputs do not feature fundamental frequency components. This permits the cancellation at the dc terminals of the circulating currents, which is achieved by inducing reactive power flows in the other two phase-legs using the orthogonality principle in the matrix $\mathbf{M}$ [23].

$$\mathbf{M} = \begin{bmatrix} \cos(\theta_L) & \frac{-\sin(\theta_L)}{\sqrt{3}} & \frac{\sin(\theta_L)}{\sqrt{3}} \\ \frac{\sin\left(\theta_L - \frac{2\pi}{3}\right)}{\sqrt{3}} & \cos\left(\theta_L - \frac{2\pi}{3}\right) & \frac{-\sin\left(\theta_L - \frac{2\pi}{3}\right)}{\sqrt{3}} \\ \frac{-\sin\left(\theta_L + \frac{2\pi}{3}\right)}{\sqrt{3}} & \frac{\sin\left(\theta_L + \frac{2\pi}{3}\right)}{\sqrt{3}} & \cos\left(\theta_L + \frac{2\pi}{3}\right) \end{bmatrix} \tag{10}$$

where θ_L is the angle of $\mathbf{e}^{\star}_L$. The vertical balancing control scheme is presented in Fig. 6. The interpretation of the first row of the matrix $\mathbf{M}$ is illustrated in Fig. 7.

This article has been accepted for publication in a future issue of this journal, but has not been fully edited. Content may change prior to final publication. Citation information: DOI 10.1109/TPEL.2018.2865422, IEEE Transactions on Power Electronics

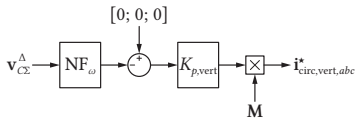

Fig. 6. Vertical balancing in abc frame, with notch filter at fundamental frequency and **M** the matrix that creates reactive power flows in the neighbouring phase-legs when a non-zero circulating current for vertical balancing is required in one phase-leg.

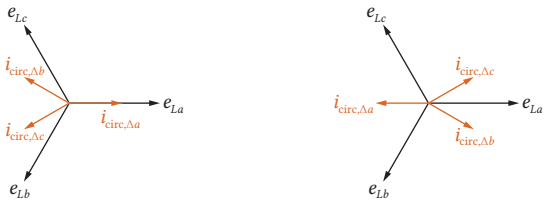

Fig. 7. Reactive currents creation to achieve cancellation on the dc bus: (a) positive case and (b) negative case of a required action for the vertical balancing in phase-leg a. The quadrature in phase-legs b and c is clearly visible.

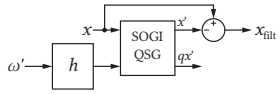

Fig. 8. Frequency adaptive notch filter based on SOGI, with a center frequency $h\omega'$.

The notch filters are implemented with a second-order generalized integrator (SOGI) structure (cf. Fig. 8), since the transfer function

$$G_{\text{SOGI}}(s) = \frac{x'(s)}{x(s)} = \frac{k\omega' s}{s^2 + k\omega' s + \omega'^2} \tag{11}$$

is a frequency adaptive bandpass filter. The quadrature signal qx' is discarded and of no use.

2) Circulating current control (CCC): While the control of the circulating currents was not considered in a first place (with very low L_{br}) [24], it has become clear that for larger values of L_{br}, also to better control the harmonic content of the branch current and eventually the branch energies, the use of a circulating current controller would be beneficial / mandatory.

The circulating current is known to naturally feature in steady state even harmonics (especially 2nd and 4th harmonics), due to the instantaneous capacitor voltage mismatch between the positive and negative branch, and odd harmonics during transients for the re-balancing of the branch energies (vertical balancing). Consequently, the circulating current controller, in its minimum configuration, should aim at suppressing undesired harmonics in the circulating current. This is what the circulating current suppression controller (CCSC) initially proposed in [25] aims at. The circulating currents can be transformed in a dq frame rotating at $-2\omega_1$ (negative sequence).

Alternatively, the circulating currents are transformed in $\alpha\beta$ frame (the zero sequence responsible for power exchange with the dc terminals is left uncontrolled) and driven to $[0\ 0]^T$ with multiple PR controllers (on 2nd and 4th harmonic for good results, especially with common mode (CM) injection) [26].

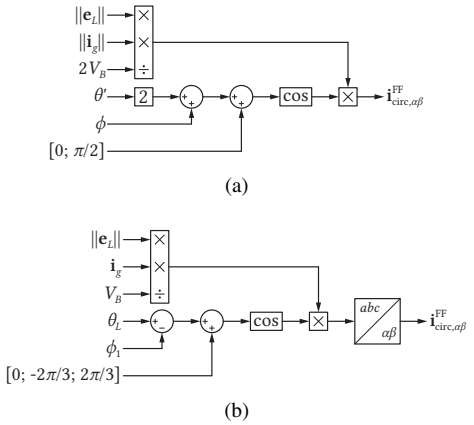

Fig. 9. Second harmonic circulating current injection (negative sequence) for capacitor voltage ripple reduction: (a) implementation that only considers the $\alpha\beta$ components, where $\phi = \text{atan}(Q^\star/P^\star)$, and (b) instantaneous power mode in [27] where the zero sequence component is discarded (usually the active power feed-forward is faster). Note that there shouldn't be any phase advance in the feed-forward term, hence $\phi_1 = \omega_1 T_d$ is subtracted to $\theta_L = \text{atan}\left(e^\star_{L,\beta}/e^\star_{L,\alpha}\right)$.

For any control method that doesn't rely on energy or voltage controllers, the odd harmonics (especially the fundamental) of the circulating current are left uncontrolled. Else, the re-balancing and long term stability would be compromised. For closed-loop modulation, where energy controllers are present, a control of the fundamental circulating current is added for improved vertical balancing performance.

$$e^\star_{B,0} = V_B - \left(k_{p,\text{ccc}} + \frac{K_{i,\text{ccc}}}{s}\right)\left(i^\star_{\text{circ},0} - i_{\text{circ},0} + i^{\text{FF}}_{\text{circ},0}\right) \tag{12a}$$

$$\mathbf{e}^\star_{B,\alpha\beta} = \left(K_{p,\text{ccc}} + \sum_{h=1,2,4} K_{h,\text{ccc}} \frac{s}{s^2 + (h\omega_1)^2}\right)\left(\mathbf{i}^\star_{\text{circ},\alpha\beta} - \mathbf{i}^\star_{\text{circ},\alpha\beta} + \mathbf{i}^{\text{FF}}_{\text{circ},\alpha\beta}\right) \tag{12b}$$

It is generally desired to use a filtered active power feed-forward ($i^{\text{FF}}_{\text{circ},0} = P^{\star\text{F}}/(3V_B)$) or just the instantaneous active power ($i^{\text{FF}}_{\text{circ},0} = P/(3V_B)$) in case the grid current control is slow. An optional second harmonic circulating current ($\mathbf{i}^{\text{FF}}_{\text{circ},\alpha\beta}$) is added with the scheme of Fig. 9. There, despite considering only a 2nd harmonic component, the ripple reduction is still achieved ($v^{\Sigma}_{C\Sigma}$ tends to a dc value).

IV. Modulation Indices Calculation

Normally, as in any converter, the modulation indices are computed with respect to the measured summed branch capacitor voltages. Therefore, eventual low order harmonics are compensated for. In the case of MMC, it was found that there might be some advantages by not using the measured summed branch capacitor voltages as is, i.e. by replacing the measurements by desired, estimated or filtered values. For these cases, no energy controllers are required. In order to allow the branch energies to self re-balance, the CCC shouldn't include an integrator on the dc component, nor resonant parts at odd multiples of the fundamental frequency.

This article has been accepted for publication in a future issue of this journal, but has not been fully edited. Content may change prior to final publication. Citation information: DOI 10.1109/TPEL.2018.2865422, IEEE Transactions on Power Electronics

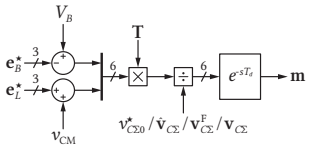

Fig. 10. Modulation indices calculation, where the term in the division is adapted depending on the modulation method.

The calculation of the modulation indices is performed according to Fig. 10, with $\mathbf{T}$ defined by (13).

$$\mathbf{T} = \begin{bmatrix} 1/2 & 0 & 0 & -1 & 0 & 0 \\ 1/2 & 0 & 0 & 1 & 0 & 0 \\ 0 & 1/2 & 0 & 0 & -1 & 0 \\ 0 & 1/2 & 0 & 0 & 1 & 0 \\ 0 & 0 & 1/2 & 0 & 0 & -1 \\ 0 & 0 & 1/2 & 0 & 0 & 1 \end{bmatrix} \tag{13}$$

A. Methods

1) Direct modulation: A formal proof regarding the self-balancing was presented in [28]. The branch modulation indices are calculated from their desired (dc) average value:

$$\mathbf{m}_p = \frac{V_B/2 - \mathbf{e}_B^\star/2 - \mathbf{e}_L^\star}{v^\star_{C\Sigma 0}} \tag{14a}$$

$$\mathbf{m}_n = \frac{V_B/2 - \mathbf{e}_B^\star/2 + \mathbf{e}_L^\star}{v^\star_{C\Sigma 0}} \tag{14b}$$

where $v^\star_{C\Sigma 0} = v^{\Sigma\star}_{C\Sigma 0}/2$. As a consequence, since the required control action for the circulating current control is assumed to be small (in steady state), the modulation indices are almost only constructed from the grid voltage component.

2) Open-loop control: The open-loop control was proposed in [12] as an improvement over the direct modulation. The motivation was double: (i) to avoid the measurement delays associated with the retrieval of the summed branch capacitor voltages and (ii) to lower the number of exchanged signals between the cells and the central controller. The common denominator from the direct modulation is replaced with the branch capacitor voltage estimates (denoted with $\hat{\cdot}$ hereafter). Therefore, the ripples are captured effectively in steady state, which is beneficial for harmonic rejection. The branch modulation indices are calculated as:

$$\mathbf{m}_p = \frac{V_B/2 - \mathbf{e}_B^\star/2 - \mathbf{e}_L^\star}{\hat{\mathbf{v}}_{C\Sigma p}} \tag{15a}$$

$$\mathbf{m}_n = \frac{V_B/2 - \mathbf{e}_B^\star/2 + \mathbf{e}_L^\star}{\hat{\mathbf{v}}_{C\Sigma n}} \tag{15b}$$

where $\hat{\mathbf{v}}_{C\Sigma p}$ and $\hat{\mathbf{v}}_{C\Sigma n}$ are obtained from Fig. 11a. The band-pass filters are implemented with a low frequency selectivity: $\alpha_f = 50\,\mathrm{rad/s}$ (similar to the PLL bandwidth). Consequently, the filters are not dependent on the frequency retrieved from the PLL, but simply from the centre grid frequency ω_1.

$$\mathrm{BPF}_h(s) = \frac{\alpha_f s}{s^2 + \alpha_f s + (h\omega_1)^2} \tag{16}$$

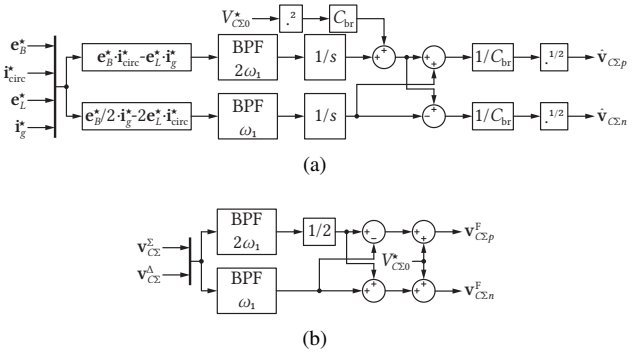

Fig. 11. Capacitor voltage ripple reconstruction methods: (a) by estimation with the open-loop control method and (b) by filtering with the hybrid voltage control method. The scaling of $\mathbf{e}_B^\star$ differs from [12] due to different scaling factors. The time-delay compensation is inherently achieved if the reference signals are properly handling delay compensation.

The formal asymptotic stability proof was provided in [29]. Note that in this case an active damping contribution to the circulating current control was added, hence the approach is not fully open-loop anymore.

3) Hybrid voltage control: Instead of the summed capacitor voltages estimates, the voltage ripples are retrieved from the measurements, while the dc part is selected the same way as for the direct modulation ($\mathbf{v}^{\mathrm{F}}_{C\Sigma p/n} = V^\star_{C\Sigma 0} + \tilde{\mathbf{v}}_{C\Sigma p/n}$). It is a compromise between the direct modulation and open-loop control, since it enables the rejection of harmonics at the terminals and achieves asymptotic stability (proven in [13]). Since the measurements are used as an input in Fig. 11b, delay compensation has to be implemented in the filters.

$$\mathbf{m}_p = \frac{V_B/2 - \mathbf{e}_B^\star/2 - \mathbf{e}_L^\star}{\mathbf{v}^{\mathrm{F}}_{C\Sigma p}} \tag{17a}$$

$$\mathbf{m}_n = \frac{V_B/2 - \mathbf{e}_B^\star/2 + \mathbf{e}_L^\star}{\mathbf{v}^{\mathrm{F}}_{C\Sigma n}} \tag{17b}$$

B. Closed-loop control

The modulation indices are computed with respect to the actual (measured) summed branch capacitor voltages, which have to be communicated to the central controller.

$$\mathbf{m}_p = \frac{V_B/2 - \mathbf{e}_B^\star/2 - \mathbf{e}_L^\star}{\mathbf{v}_{C\Sigma p}} \tag{18a}$$

$$\mathbf{m}_n = \frac{V_B/2 - \mathbf{e}_B^\star/2 + \mathbf{e}_L^\star}{\mathbf{v}_{C\Sigma n}} \tag{18b}$$

C. Discussion

In HVdc applications, the closed-loop control method clearly suffers from implementation complexity, since all the cell capacitor voltages have to be measured, aggregated and communicated to the central controller within reasonable time delays. For MVdc applications with a much lower number of cells per branch, this is not considered as a large concern, especially if the branch or phase-leg modulation is performed at an intermediate level, between the cell controller and the central controller. To support this discussion, a decentralized modulation with a closed-loop control of the branch energies has been implemented in [30]. No large penalty from the time delays on the converter dynamics is reported.

This article has been accepted for publication in a future issue of this journal, but has not been fully edited. Content may change prior to final publication. Citation information: DOI 10.1109/TPEL.2018.2865422, IEEE Transactions on Power Electronics

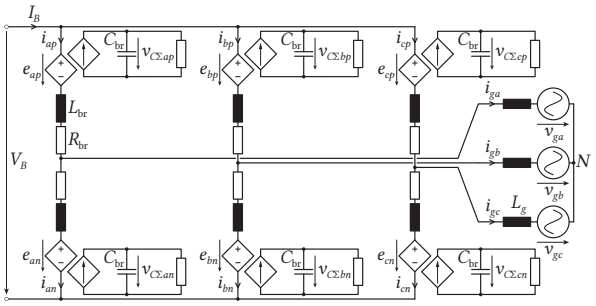

Fig. 12. Dc/3-ac MMC average model scheme and nomenclature.

V. MVdc benchmark simulations

While the presented methods have been reported in the literature, it is very hard to directly compare them, as different groups of authors have used different system ratings or considered different applications. Each control method has been implemented in PLECS. In order to provide a fair comparison of their performances, the converter model and controller parameters are identical among all models, at the exception of the direct modulation without circulating current control. It is only present to motivate for the use of a CCC. Note that MV applications are expected to feature faster dynamics than the HVdc ones. A connection to a $10\,\mathrm{kV_{dc}}$ link is considered. Realistic designs, e.g. based on $1.7\,\mathrm{kV}$ semiconductors for a good trade-off between conduction and switching losses, would result in around 8 cells per branch.

A. Converter model

Since the number of cells per branch is reduced compared to HVdc designs, PWM methods with an average cell switching frequency in the range of a few hundreds of Hz is assumed. In order to avoid interactions with the modulation methods, a branch average model rather than a switched one was selected. The model is inspired from [31], [32]. Such a model is a simplification from (3), since all individual cell capacitor voltages are aggregated together. In this work, quantization effects are neglected, even though they might not be completely negligible, especially at low average branch switching frequencies / low cell numbers [33]. The time delays, which play a fundamental role in the limitation of the control gains, are modelled by a pure time delay with a total value T_d in (19). It is hardly possible to come up with a value for T_d that fits all possible control hardware implementations. This is considered out of the scope of this paper and the value provided is considered reasonable. The dc/3-ac MMC model with the considered branch average model is shown in Fig. 12.

$$e_{xy} = m_{xy} e^{-sT_d} v_{C\Sigma xy} \tag{19a}$$

$$i_{\Sigma xy} = m_{xy} e^{-sT_d} i_{xy} \tag{19b}$$

B. Controller parameters

A fair comparison between the different modulation indices calculation methods is performed with identical controller tunings. The system and control parameters are given in Table I and Table II, respectively. A strong ac grid is considered (infinite short-circuit ratio (SCR)). In case of weak grids (SCR < 10), the voltage at the PCC should be controlled (closed-loop reactive power control). Such a case was not considered relevant regarding the objective of this work: the comparison of the inner state variable control. The two converter modes are analysed separately.

TABLE I: System parameters.

Parameter	Value
$v_{g,ll}$	$5.2\,\mathrm{kV}$ (1 p.u.)
f_g	$50\,\mathrm{Hz}$ (1 p.u.)
S	$0.5\,\mathrm{MVA}$ (1 p.u.)
Z_b	$54\,\Omega$ (1 p.u.)
V_{dc}	$10\,\mathrm{kV}$ (1.92 p.u.)
L_{br}	$2.5\,\mathrm{mH}$ (0.0145 p.u.)
R_{br}	$0.1\,\Omega$ (0.0019 p.u.)
C_{br}	$118.75\,\mu\mathrm{F}$ (0.49 p.u.)
L_g	$0\,\mathrm{H}$
R_g	$0\,\Omega$
$f_{\mathrm{sw,app}}$	$5\,\mathrm{kHz}$
T_d	$1.5/f_{\mathrm{sw,app}}$

TABLE II: Controller parameters.

Controller	Parameter	Value
PLL	$\alpha_{p,\mathrm{PLL}}$	$50\,\mathrm{rad/s}$
	$\alpha_{ip,\mathrm{PLL}}$	$10\,\mathrm{rad/s}$
GCC	α_{GCC}	$2\pi f_{\mathrm{sw,app}}/10$
	$\alpha_{h,\mathrm{GCC}}$	$200\,\mathrm{rad/s}$
CCC	α_{CCC}	$\alpha_{\mathrm{GCC}}/2$
	$\alpha_{h,\mathrm{CCC}}$	$100\,\mathrm{rad/s}$
DVC	α_d	$50\,\mathrm{rad/s}$
	α_{id}	$25\,\mathrm{rad/s}$
ΣVC	α_{hor}	$\alpha_{\mathrm{CCC}}/10$
	$\alpha_{h,\mathrm{hor}}$	$1\,\mathrm{rad/s}$
ΔVC	α_{vert}	$\alpha_{\mathrm{CCC}}/10$
LPF	$\alpha_{v^\star_{C\Sigma 0}}$	$20\,\mathrm{rad/s}$
BPF	α_f	$50\,\mathrm{rad/s}$

C. Converter safe operating areas (SOAs)

During the design and sizing of an MMC, it is important to address the SOA of the converter. The converter's SOA is more representative than the cell's SOA, which defined by a current limit (linked to the cooling capacity) and a voltage limit (what is the highest voltage the cell's capacitors can handle). In addition, the harmonic content of the branch currents and voltages have a non negligible impact that one has to be aware of. The corresponding SOAs for the considered converter design are shown in Fig. 13. They were obtained by evaluating the analytical model of the converter inspired from the power equations [34], which means that they do not consider control dynamics (such as overshoots, etc.), but solely steady state operating points. The limits are set by: $v_{C\Sigma} \in [0.9V_{\mathrm{dc}},\ 1.1V_{\mathrm{dc}}]$, $i_{\mathrm{br}} \in [-70\,\mathrm{A},\ 70\,\mathrm{A}]$, $m \in [0,\ 1]$, which correspond to the converter prototype under construction [35]–[37].

The operation with a purely dc circulating current is greatly advantageous compared to the case with 2^{nd} (+ 4^{th}) harmonic circulating current injection, especially given the low branch

This article has been accepted for publication in a future issue of this journal, but has not been fully edited. Content may change prior to final publication. Citation information: DOI 10.1109/TPEL.2018.2865422, IEEE Transactions on Power Electronics

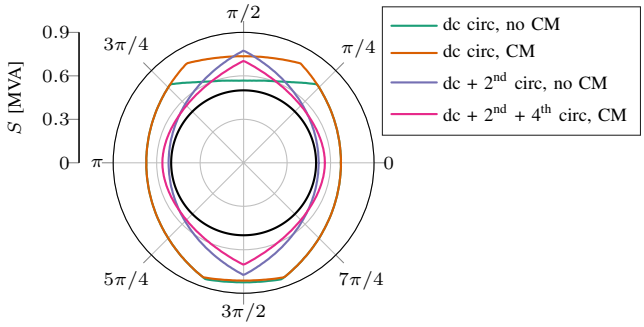

Fig. 13. MMC SOAs derived from the power equations without passives with $C_{\text{br}} = 118.75\,\mu\text{F}$. The black circle corresponds to $S = 0.5\,\text{MVA}$.

TABLE III: Control method comparison configurations in inverter mode. A filled dot corresponds to the presence of a CCC, CM voltage or 2nd harmonic circulating current injection, and the absence for an unfilled one.

Case #	Control method	CCC	CM	2nd circ
1	Direct modulation	○	○	○
2	Direct modulation	●	○	○
3	Direct modulation	●	○	●
4	Open-loop control	●	○	○
5	Hybrid voltage control	●	○	○
6	Closed-loop control	●	○	○

current limits (thermal limit). For load angles close to $\pi/2$, the CM injection is highly beneficial, since it displaces the intersection between the peak of the branch voltage and the summed branch capacitor voltage, which is limiting the SOA in this region when no CM is present. Note that the choice of the CM injection method (sine, min/max, flat-top [38]) has a negligible influence on the converter SOA.

D. Inverter mode

The typical applications for an MMC in inverter mode is the converter station at the end of a dc transmission, when active power is transferred from the dc to the ac grid. Alternatively, it could also be the case for a (high speed) motor drive. The complete overall control scheme is shown in Fig. 2a. Six cases are compared, and their configurations are summarized in Table III. Each control method is evaluated with a dc circulating current. Note that in order to maintain a reasonable number of cases, the CM and harmonic circulating current injections were discarded.

1) Current control and harmonic content: The obtained currents are shown in Fig. 14 for each case of Table III. In order to provide an additional insight in their harmonic content, Fig. 15 shows their FFT for a two fundamental periods window with only active power injection.

In direct modulation without CCC (cf. Fig. 14a), the circulating current features several low order even harmonics (2nd, 4th, etc). The bus current I_B features a strong 6th harmonic ripple component (around $1\,\%$ of the dc current). The grid current features 5th and 7th harmonics (cf. Fig. 15a). Once a CCSC is added (cf. Fig. 14b), even though it is not tuned very aggressively ($\alpha_{h,\text{CCC}} = 100\,\text{rad/s}$), it can be observed that the harmonics in the circulating current decay slowly at

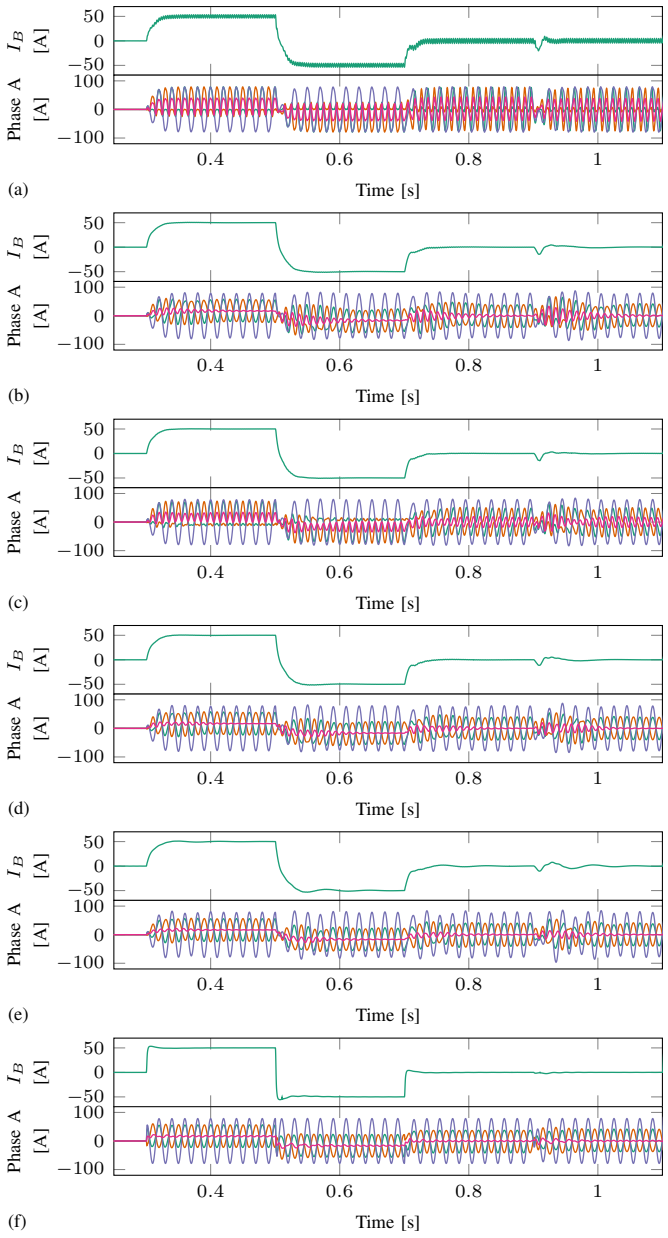

Fig. 14. Currents in inverter mode: (a) direct modulation without CCSC, (b) direction modulation with CCSC, (c) direct modulation with CCSC and 2nd harmonic circulating current injection, (d) open-loop control, (e) hybrid voltage control and (f) closed-loop control. The color scheme for the bottom plots is: i_{ap} in green, i_{an} in red, i_{ga} in blue and $i_{\text{circ},a}$ in pink.

each power step (around 8 fundamental periods). As a consequence, the low order harmonics at the terminals disappear in steady state (cf. Fig. 15b). From there, the dynamics can be slightly improved by injecting a 2nd harmonic circulating current (cf. Fig. 14c, around 3 fundamental periods). The open-loop modulation with CCSC (cf. Fig. 14d) is similar to the direct modulation in terms of dynamics of the dc bus current, however a faster decay in the circulating current is observed (around 6 fundamental periods), thanks to the reconstructed capacitor voltage ripples. The hybrid voltage control with CCSC (cf. Fig. 14e) has worse dynamics compared to the open-loop control. This is a consequence of the band-pass filters, which are effective in steady state, but feature large delays during

This article has been accepted for publication in a future issue of this journal, but has not been fully edited. Content may change prior to final publication. Citation information: DOI 10.1109/TPEL.2018.2865422, IEEE Transactions on Power Electronics

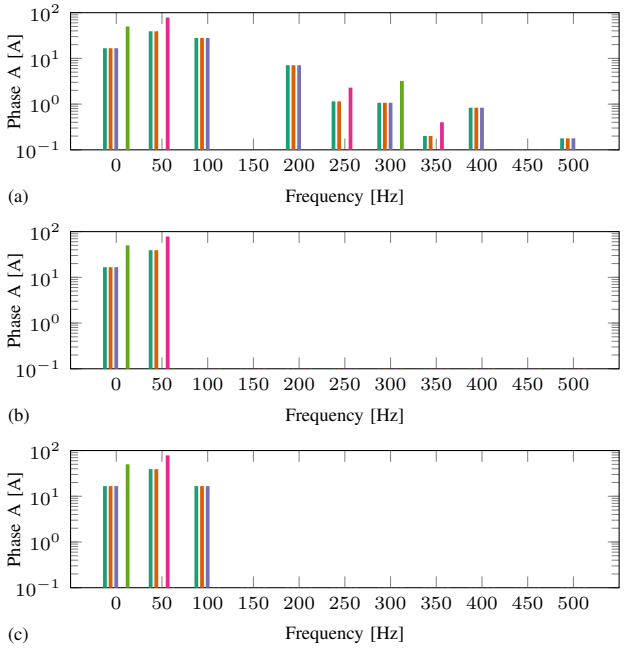

Fig. 15. FFT in a two fundamental periods window between 1.9 and 1.94 s where $P^\star = 0.5\,\mathrm{MVA}$: (a) direct modulation without CCSC, (b) CCC with dc circulating current, (c) CCC with 2nd harmonic injection. The colour scheme is: i_{ap} in dark green, i_{an} in red, $i_{\mathrm{circ},a}$ in blue, i_{ga} in pink and I_B in light green.

transients. The dc current has oscillations with low damping. Finally, the closed-loop modulation (cf. Fig. 14f) has the best dynamic performances. The 2nd harmonic circulating current is not totally removed since the circulating current reference from the horizontal balancing contains a small 2nd harmonic component, but the current transients are fast (below one fundamental period).

In a nutshell, it is concluded that a CCC is needed to get control over the low order harmonics at the terminals. Then, depending on the degree of accuracy of the capacitor voltage ripples reproduction, different dynamics are observed.

2) Capacitor voltages: The result for the summed branch capacitor voltages is shown in Fig. 16. In the case of the direct modulation without CCC, due to the large circulating current for rebalancing the branch energies, the capacitor voltage ripples are the lowest amongst all control methods. On the other hand, due to the absence of capacitor voltage controllers, their average is offset during reactive power transients (cf. Fig. 16a). A similar behaviour is observed for the open-loop and hybrid voltage controls (cf. Fig. 16d and (e)). When a 2nd harmonic circulating current is injected, the ripples in $\mathbf{v}_{C\Sigma}^{\Sigma}$ are almost completely removed (cf. Fig. 16c). Due to the inherent self-balancing capability, no large rebalancing in $\mathbf{v}_{C\Sigma}^{\Delta}$ is observed. However, the response of $\mathbf{v}_{C\Sigma}^{\Sigma}$ shows an oscillatory response, in particular with the hybrid voltage control (cf. Fig. 16e), leading to large capacitor voltage deviations during transients. This observation tends to suggest that the bandwidth of the power steps should be even further reduced for the hybrid voltage control method. For the closed-loop control, due to the capacitor voltage controllers, the rebalancing of the branch energies is slower compared to the other control methods (it

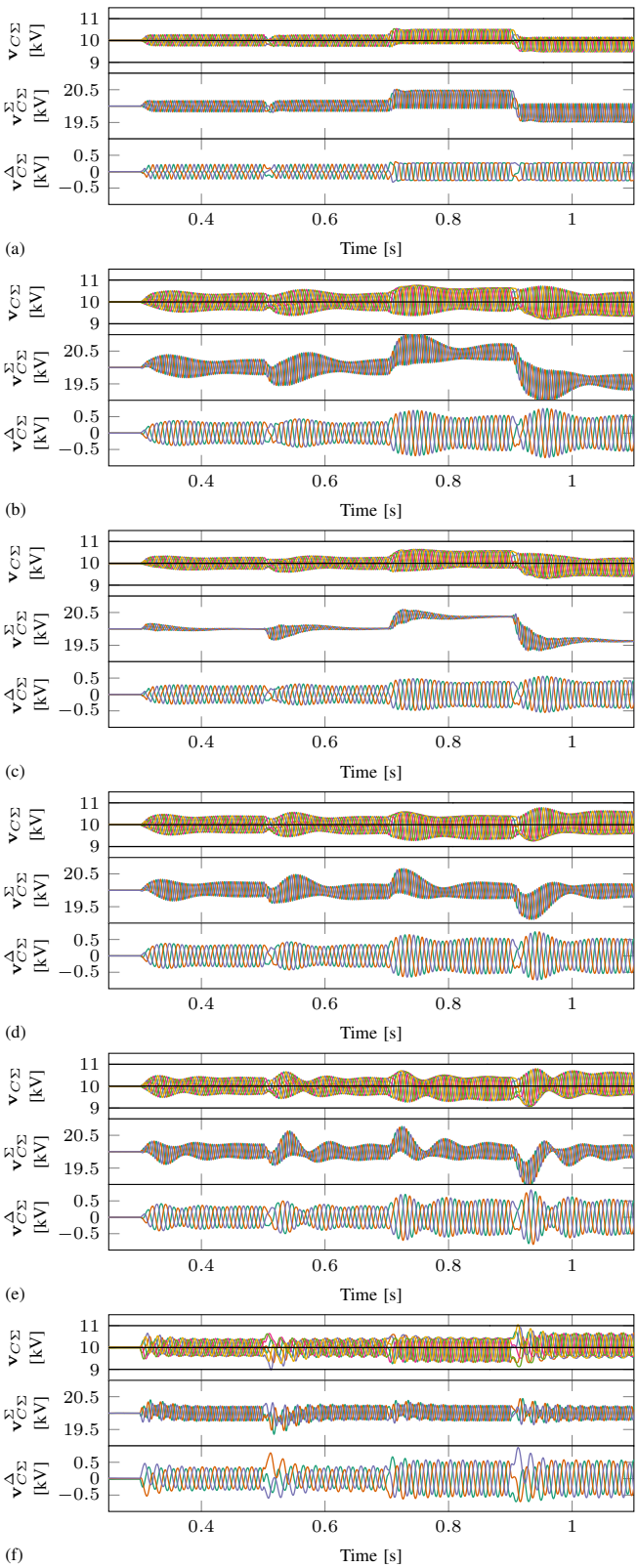

Fig. 16. Summed and transformed branch capacitor voltages in inverter mode: (a) direct modulation without CCSC, (b) direction modulation with CCSC, (c) direct modulation with CCSC and 2nd harmonic circulating current injection, (d) open-loop control, (e) hybrid voltage control and (f) closed-loop control. The transformed branch capacitor voltages follow the definition of (2b). Note that the main frequency of the ripple in $\mathbf{v}_{C\Sigma}^{\Sigma} = 2f_g$, while it is f_g for $\mathbf{v}_{C\Sigma}^{\Delta}$.

This article has been accepted for publication in a future issue of this journal, but has not been fully edited. Content may change prior to final publication. Citation information: DOI 10.1109/TPEL.2018.2865422, IEEE Transactions on Power Electronics

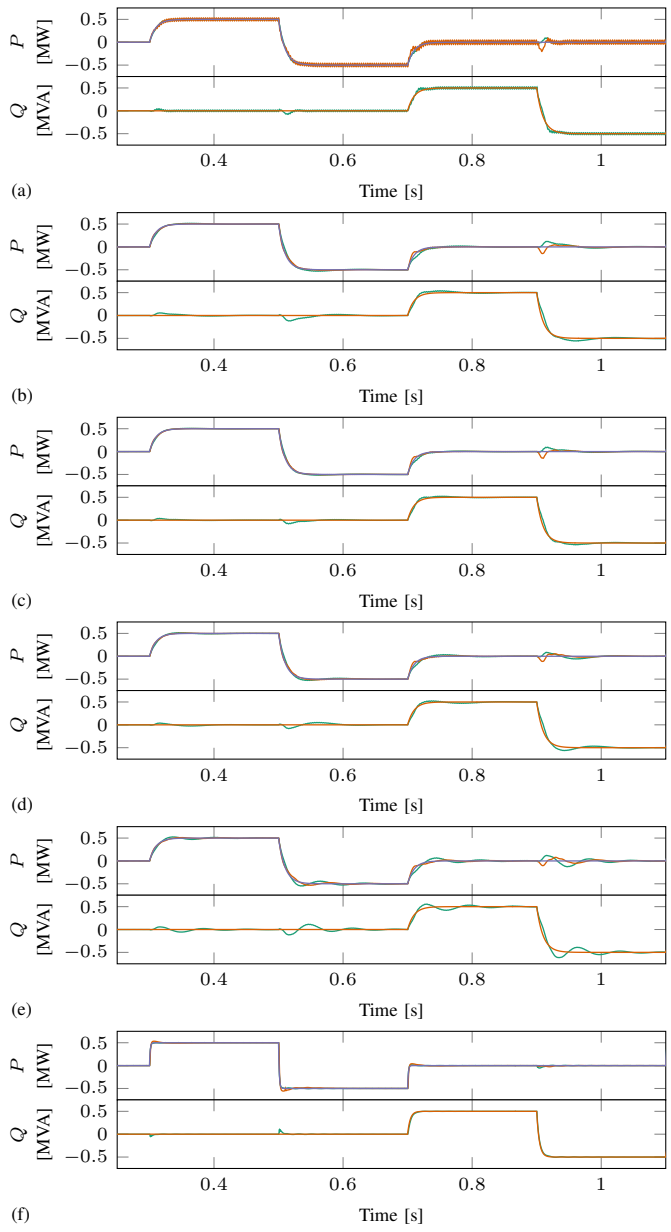

Fig. 17. PQ tracking in inverter mode: (a) direct modulation without CCSC, (b) direction modulation with CCSC, (c) direct modulation with CCSC and 2nd harmonic circulating current injection, (d) open-loop control, (e) hybrid voltage control and (f) closed-loop control. The color scheme is: P_{ac} in green, P_{dc} in red and $P^{\star\text{F}}$ in blue for the P plots and Q_{ac} in green and $Q^{\star\text{F}}$ in red for the Q ones.

TABLE IV: Control performance in rectifier mode.

Case #	Control method	CCC	CM	2nd harmonic
1	Closed-loop control	●	○	○
2	Open-loop control	●	○	○

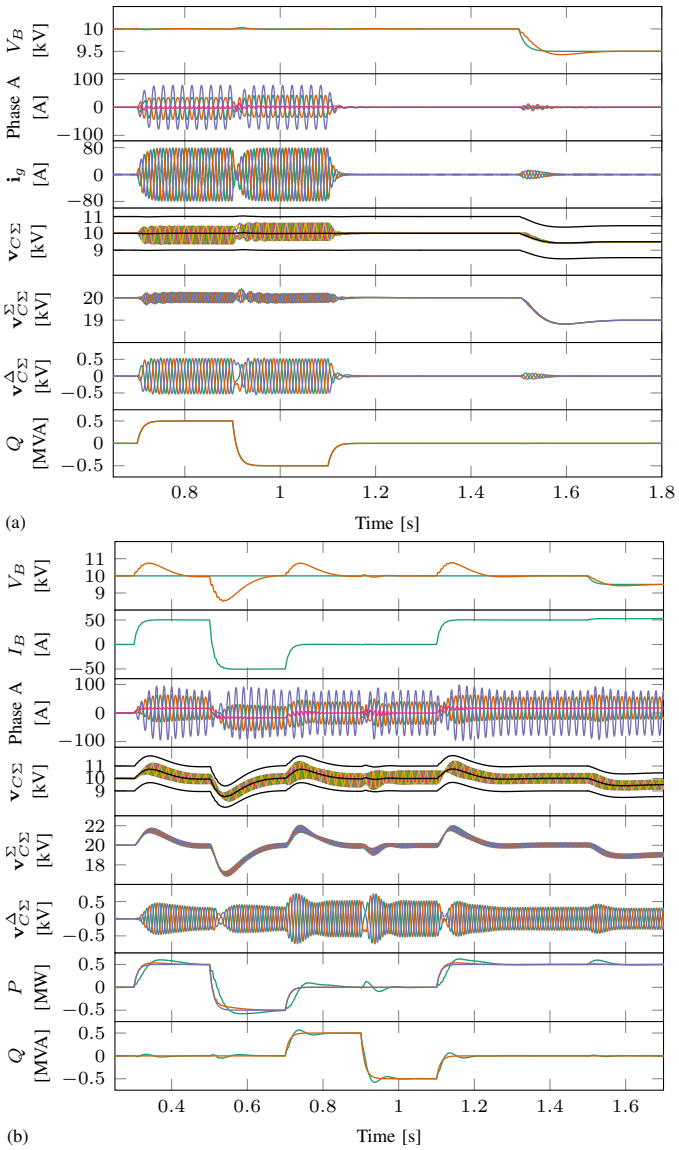

Fig. 18. MMC in rectifier mode: (a) with no load and closed-loop control (the objective is to verify that the circulating currents are cancelling at the terminals) and (b) with a current source and open-loop control. The colour scheme is $V_B^{\text{F}\star}$ in green and V_B in red.

takes 3 fundamental periods to rebalance the vertical energy with steps from 0 to the nominal value). However, it is done in a much more controlled fashion, since these unbalances do not result in power oscillations (cf. Fig. 16f).

3) PQ tracking: The PQ tracking is shown is Fig. 17, with current references set in open-loop as described in (4). The low-pass filter bandwidths are set to $100\,\text{rad/s}$ (a trade-off between the overshoot and the tracking performance). For the direct modulation without CCC, due to the presence of low order harmonics at the terminals, the measured P and Q have ripples at the same frequencies (cf. Fig. 17a). When a CCC is present, these ripples are removed. The injection of a 2nd harmonic circulating current improves the response with the direct modulation (Fig. 17b versus Fig. 17c). With the ripple reconstruction methods, the measured P and Q show an oscillatory response, particularly underdamped in the case of the hybrid voltage control, where the Q tracking is particularly poor (cf. Fig. 17e). With the closed-loop control, the low-pass filter bandwidths on P and Q are increased to $300\,\text{rad/s}$ without controller tuning optimization. Note that the powers are almost perfectly decoupled, despite some coupling visible during power steps. The major improvement with the closed-loop control is the removal of the chattering between the dc

This article has been accepted for publication in a future issue of this journal, but has not been fully edited. Content may change prior to final publication. Citation information: DOI 10.1109/TPEL.2018.2865422, IEEE Transactions on Power Electronics

and ac terminal powers, which lasts from 100 to 300 ms with the other control methods.

E. Rectifier mode

Applications considering an MMC as a rectifier range from versatile high performance dc source [30] to sending port of a dc transmission. In that operating mode, the DVC is added. The full control scheme is shown in Fig. 2b.

Since the results in inverter mode have highlighted the behaviour of the low order harmonics, the circulating current, the summed branch capacitor voltage ripples and the PQ tracking, this section restrains the comparison to the DVC only. Table IV shows the two studied cases.

In Fig. 18a, the cancellation of the circulating currents between the phase-legs is verified. Otherwise, the CCC would lead to instabilities. The performance of the DVC is ideal, since no power is drained from the dc terminal. In Fig. 18b, simulation results with a current source (with an additional 30 µF capacitor across the dc terminals) are shown. The dc dynamics are limited by the active power dynamics on the ac side, which is slow with the open-loop control (100 rad/s).

VI. Discussion

All the observations can be summarized with qualitative spider graphs shown in Fig. 19. Note that Fig. 19f is the result of the superposition of each of the five control methods (the direct modulation with CCSC is overlapping with the direct modulation with CCSC and 2nd harmonic circulating current injection). There are five gradations, shown with gray lines, from low (close to the centre) to high (at the outside). These ratings represent expert opinion on a unit-less scale, as a result of the above comprehensive study. An exact quantification is not easy and will depend on realisation and implementation means. The six representative performance indices are:

1) CCC complexity. The circulating current control require multi-frequency resonant controllers, as presented in Section III-B2. The direct modulation without CCSC has the smallest circulating current. The estimation-based methods have simpler CCC, since the dc part as well as the odd harmonics are left uncontrolled. At last, the closed-loop control method requires the complete control of the circulating currents over the low frequency range, in order for the energy balancing to perform as expected.
2) Low order harmonics at the terminal. The low order harmonics at the terminal are problematic, since they're too low in frequency to consider their cancellation with passive filters. The price to pay for the direct modulation without CCSC is that these low order harmonics are present at the terminals, which questions the relevance of this control method for any real life application. It was observed in Fig. 15 that the addition of a CCSC is sufficient to remove these critical harmonics.
3) Energy controllers. The estimation-based methods (direct modulation, open-loop control and hybrid voltage control) are characterized by their simplicity with the absence of energy controllers. Consequently, they're all graded at the minimum. On the contrary, the closed-loop control method relies on complex energy controllers (for both horizontal and vertical balancing), with a heavy implementation cost, as presented in Section III-B1. For those reasons, the largest grading is attributed to this method.
4) Digital filters. Digital filters are absent with the direct modulation. With the open-loop control, bandpass filters are present with a loose frequency selectivity. With the closed-loop control, bandpass filters are important for the energy balancing control at the level of the decoupling of the capacitor voltages for the horizontal and vertical balancing. For the hybrid voltage control, the tuning of the bandpass filters is crucial, since they govern the

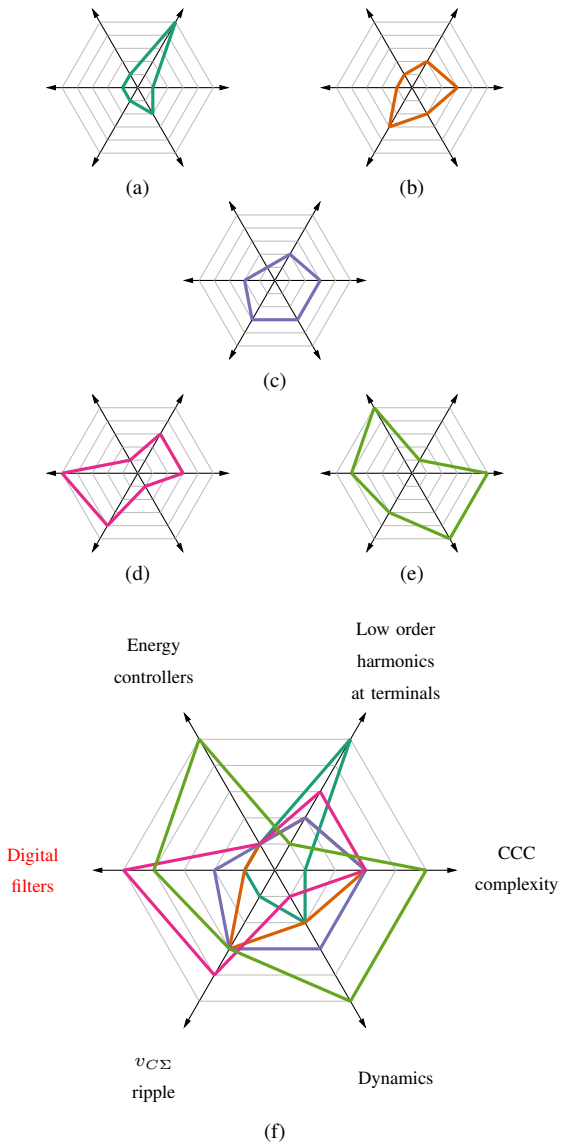

Fig. 19. Control methods benchmark: (a) – (e) individual control method performance and (f) converter performance comparison. The axes labels for (a) – (e) are identical to (f). Note that the direct modulation with CCSC is overlapping with the direct modulation with CCSC and 2nd harmonic circulating current injection. The color scheme is: direct modulation without CCC in dark green, direct modulation with CCSC in red, open-loop control in blue, hybrid voltage control in pink and closed-loop control in light green.

achievable transient performance. In that perspective, their tuning is considered very sensitive.

5) Summed capacitor voltage ripples. The estimation-based methods, due to their self-balancing property, show good performance on $\mathbf{v}_{C\Sigma}^{\Delta}$. However, large differences are visible in $\mathbf{v}_{C\Sigma}^{\Sigma}$, and this is the focus of this discussion. The direct modulation without CCSC has the highest balancing capability. The closed-loop control, through its energy balancing, has a reasonably low capacitor voltage ripple, which take three fundamental period to rebalance after a transient. The open-loop control shows smooth transients in the summed capacitor voltage ripples, with a similar duration of the rebalancing process as with the closed-loop control. As a consequence of the loosely damped power oscillations during step changes, the hybrid voltage control presents the largest summed capacitor voltage ripples.
6) Dynamics. Fig. 17 is the most relevant figure to discuss output dynamics. At first sight, the closed-loop control modulation is the fastest, since nominal power steps with a bandwidth of $300\,\mathrm{rad/s}$ is easily achievable without control parameter optimization, at the expense of a little overshoot. It is three times faster than with the other methods. As a consequence, the dynamics grade is set to the highest level. The direct modulation without CCSC comes second, with fast dynamics despite undamped power oscillations. In the third position is the direct modulation with CCSC and 2$^{\text{nd}}$ harmonic circulating current injection, with a good decoupling between the active and reactive powers, and a well damped response. Fourth comes the open-loop control, with decent dynamics but slightly less damps oscillations during the transients. At last, the hybrid voltage control struggles on fast power transients, mainly due to the delay origination from the digital bandpass filters that take quite some time to reach the new steady state. As a consequence, the oscillatory response is poorly damped and features a significant overshoot, especially on reactive power transients.

VII. Conclusion

A thorough comparison of the performances of four control methods proposed for the dc/3-ac MMC has been carried out, supported by extensive simulations on an average model to remove interactions from the modulation method on the control performances.

In any case, the need for a CCC was motivated by the comparison of the harmonic spectra in inverter mode. This is the only way to get rid of low-order harmonics at the terminals that do not make sense to be removed with passive filters while a control extension is at hand. The performances during transients is mainly governed by the accuracy of the capacitor voltage ripple reproduction. In that perspective, the open-loop control always performs better than the hybrid voltage control. The latter suffers from limited dynamics due to delays originating from the high frequency selectivity of the bandpass filters used to retrieve the voltage ripple components. In steady state, these methods perform in a comparable manner, thanks to the action of the CCSC combined with the summed capacitor voltage reconstruction that matches accurately the measured values. Similar performances are obtained with the direct modulation augmented with a CCSC. It might qualify the ripple reconstruction. However, the average model simulations do not properly highlight the impact from the modulation, since the voltage error between the desired and applied branch emf voltage ($e_{p/n}$) is much larger with direct modulation compared to the others, where the steady-state capacitor voltage ripple is either reconstructed or simply measured.

General guidelines can be introduced for MVdc applications, and the conclusions might differ from HVdc applications, since the converter designs contain few cells. For a low control complexity, in case of an application with a low dynamics requirement, the open-loop control method shall be favoured. In case of an application with high dynamics, the closed-loop control clearly outperform all the other methods, at the expense of a more complex control structure. For MVdc applications, the fast transfer of the cell's capacitor voltage measurements to the controller where the modulation is performed is not considered as a major challenge.

References

[1] R. Marquardt, A. Lesnicar, and J. Hildinger, "Modulares stromrichterkonzept für netzkupplungsanwendungen bei hohen spannungen," in *ETG-Fachtagung*, 2002.
[2] J. Gerdes, "Siemens Debuts HVDC PLUS with San Francisco's Trans Bay Cable," *Living Energy*, pp. 28–31, Jul. 2011.
[3] M. Pereira, D. Retzmann, J. Lottes, M. Wiesinger, and G. Wong, "Svc plus: An mmc statcom for network and grid access applications," in *2011 IEEE Trondheim PowerTech*, Jun. 2011, pp. 1–5.
[4] Siemens AG, *Sitras SFC PLUS*, http://www.mobility.siemens.com/mobility/global/en/interurban-mobility/rail-solutions/railway-electrification/ac-traction-power-supply/Documents/sitras-sfc-plus-en.pdf, 2016.
[5] ABB, *Rail SFC Light*, http://new.abb.com/facts/static-frequency-converters-(sfc)/rail-static-frequency-converters/rail-sfc-light.
[6] M. Hiller, S. Busse, and A. H. Gheeth, *Modular Multilevel Converter (M2C) Medium Voltage Drives: Working Principle*, Technical Paper, Siemens AG, 2016.
[7] Benshaw Inc., *Benshaw M2L 3000 MV VFD Brochure*, http://www.benshaw.com/WorkArea/DownloadAsset.aspx?id=97, 2017.
[8] Siemens AG, *SIHARBOR*, https://w3.siemens.com/powerdistribution/global/en/mv/power-supply-solutions/onshore-power-supply/pages/siharbor.aspx.
[9] ——, *MVDC PLUS*, https://www.siemens.com/global/en/home/products/energy/medium-voltage/solutions/mvdc.html.
[10] RXPE, *Smart VSC-MVDC Transmission*, http://www.rxpe.co.uk/solutions/smart-vsc-hvdc-transmission/smart-vsc-mvdc-transmission/.
[11] C. Oates, "A methodology for developing chainlink converters," in *2009 13th European Conference on Power Electronics and Applications*, Sep. 2009, pp. 1–10.
[12] L. Angquist, A. Antonopoulos, D. Siemaszko, K. Ilves, M. Vasiladiotis, and H. P. Nee, "Open-loop control of modular multilevel converters using estimation of stored energy," *IEEE Transactions on Industry Applications*, vol. 47, no. 6, pp. 2516–2524, Nov. 2011.
[13] L. Harnefors, A. Antonopoulos, K. Ilves, and H. P. Nee, "Global asymptotic stability of current-controlled modular multilevel converters," *IEEE Transactions on Power Electronics*, vol. 30, no. 1, pp. 249–258, Jan. 2015.
[14] G. Bergna, E. Berne, P. Egrot, P. Lefranc, A. Arzande, J. C. Vannier, and M. Molinas, "An energy-based controller for hvdc modular multilevel converter in decoupled double synchronous reference frame for voltage oscillation reduction," *IEEE Transactions on Industrial Electronics*, vol. 60, no. 6, pp. 2360–2371, Jun. 2013.
[15] "Ieee draft recommended practice for 1 kv to 35 kv medium-voltage dc power systems on ships," *IEEE P1709/D5, January 2018*, pp. 1–48, Jan. 2018.

[16] Cigré, *Working Group C6.31: Medium Voltage Direct Current (MVDC) Grid Feasibility Study*, http://c6.cigre.org/WG-Area/WG-C6.31-Medium-Voltage-Direct-Current-MVDC-Grid-Feasibility-Study, 2016.

[17] N. Cherix, "Functional description and control design of modular multilevel converters towards energy storage applications for traction networks," PhD thesis, École Polytechnique Fédérale de Lausanne, 2015.

[18] H. Akagi, E. H. Watanabe, and M. Aredes, "The instantaneous power theory," in *Instantaneous Power Theory and Applications to Power Conditioning*. Wiley-IEEE Press, 2017.

[19] D. N. Zmood and D. G. Holmes, "Stationary frame current regulation of pwm inverters with zero steady-state error," *IEEE Transactions on Power Electronics*, vol. 18, no. 3, pp. 814–822, May 2003.

[20] A. Yazdani and R. Iravani, "An accurate model for the dc-side voltage control of the neutral point diode clamped converter," *IEEE Transactions on Power Delivery*, vol. 21, no. 1, pp. 185–193, Jan. 2006.

[21] A. Antonopoulos, L. Angquist, and H. P. Nee, "On dynamics and voltage control of the modular multilevel converter," in *2009 13th European Conference on Power Electronics and Applications*, Sep. 2009, pp. 1–10.

[22] J. Kolb, F. Kammerer, M. Gommeringer, and M. Braun, "Cascaded control system of the modular multilevel converter for feeding variable-speed drives," *IEEE Transactions on Power Electronics*, vol. 30, no. 1, pp. 349–357, Jan. 2015.

[23] P. Münch, D. Görges, M. Izák, and S. Liu, "Integrated current control, energy control and energy balancing of modular multilevel converters," in *IECON 2010 - 36th Annual Conference on IEEE Industrial Electronics Society*, Nov. 2010, pp. 150–155.

[24] S. Rohner, S. Bernet, M. Hiller, and R. Sommer, "Analysis and simulation of a 6 kv, 6 mva modular multilevel converter," in *2009 35th Annual Conference of IEEE Industrial Electronics*, Nov. 2009, pp. 225–230.

[25] Q. Tu, Z. Xu, and L. Xu, "Reduced switching-frequency modulation and circulating current suppression for modular multilevel converters," *IEEE Transactions on Power Delivery*, vol. 26, no. 3, pp. 2009–2017, Jul. 2011.

[26] X. She, A. Huang, X. Ni, and R. Burgos, "Ac circulating currents suppression in modular multilevel converter," in *IECON 2012 - 38th Annual Conference on IEEE Industrial Electronics Society*, Oct. 2012, pp. 191–196.

[27] M. Winkelnkemper, A. Korn, and P. Steimer, "A modular direct converter for transformerless rail interties," in *Industrial Electronics (ISIE), 2010 IEEE International Symposium on*, Jul. 2010, pp. 562–567.

[28] S. Cui, J. J. Jung, Y. Lee, and S. K. Sul, "Principles and dynamics of natural arm capacitor voltage balancing of a direct modulated modular multilevel converter," in *2015 9th International Conference on Power Electronics and ECCE Asia (ICPE-ECCE Asia)*, Jun. 2015, pp. 259–267.

[29] A. Antonopoulos, L. Ängquist, L. Harnefors, K. Ilves, and H. P. Nee, "Global asymptotic stability of modular multilevel converters," *IEEE Transactions on Industrial Electronics*, vol. 61, no. 2, pp. 603–612, Feb. 2014.

[30] M. M. Steurer, K. Schoder, O. Faruque, D. Soto, M. Bosworth, M. Sloderbeck, F. Bogdan, J. Hauer, M. Winkelnkemper, L. Schwager, and P. Blaszczyk, "Multifunctional megawatt-scale medium voltage dc test bed based on modular multilevel converter technology," *IEEE Transactions on Transportation Electrification*, vol. 2, no. 4, pp. 597–606, Dec. 2016.

[31] S. Rohner, J. Weber, and S. Bernet, "Continuous model of modular multilevel converter with experimental verification," in *2011 IEEE Energy Conversion Congress and Exposition*, Sep. 2011, pp. 4021–4028.

[32] D. C. Ludois and G. Venkataramanan, "Simplified terminal behavioral model for a modular multilevel converter," *IEEE Transactions on Power Electronics*, vol. 29, no. 4, pp. 1622–1631, Apr. 2014.

[33] A. Lopez, D. E. Quevedo, R. P. Aguilera, T. Geyer, and N. Oikonomou, "Limitations and accuracy of a continuous reduced order model for modular multilevel converters," *IEEE Transactions on Power Electronics*, vol. PP, no. 99, pp. 1–1, 2017.

[34] M. Vasiladiotis, N. Cherix, and A. Rufer, "Accurate capacitor voltage ripple estimation and current control considerations for grid-connected modular multilevel converters," *Power Electronics, IEEE Transactions on*, vol. 29, no. 9, pp. 4568–4579, Sep. 2014.

[35] E. Coulinge, A. Christe, and D. Dujic, "Electro-thermal design of a modular multilevel converter prototype," in *PCIM Europe 2016; International Exhibition and Conference for Power Electronics, Intelligent Motion, Renewable Energy and Energy Management*, May 2016, pp. 1–8.

[36] A. Christe and D. Dujic, "Galvanically isolated modular converter," *IET Power Electronics*, vol. 9, no. 12, pp. 2318–2328, 2016.

[37] ——, "Virtual submodule concept for fast semi-numerical modular multilevel converter loss estimation," *IEEE Transactions on Industrial Electronics*, vol. 64, no. 7, pp. 5286–5294, Jul. 2017.

[38] R. Li, J. E. Fletcher, L. Xu, and B. W. Williams, "Enhanced flat-topped modulation for mmc control in hvdc transmission systems," *IEEE Transactions on Power Delivery*, vol. 32, no. 1, pp. 152–161, Feb. 2017.

Alexandre Christe (S'14) received the B.Sc., M.Sc. and PhD degrees in electrical engineering from the École Polytechnique Fédérale de Lausanne (EPFL), Lausanne, Switzerland, in 2012, 2014 and 2018, respectively.

From April 2014 till March 2018, he was with the Power Electronics Laboratory as a doctoral assistant. Since May 2018, he joined ABB Corporate Research Center, Västerås, Sweden, as a Scientist.

His research interests include the design, control and modulation of multilevel converters for medium voltage applications.

Drazen Dujic (S'03-M'09-SM'12) received the Dipl.-Ing. and M.Sc. degrees from University of Novi Sad, Novi Sad, Serbia, in 2002 and 2005, respectively, and the Ph.D. degree from Liverpool John Moores University, Liverpool, U.K., in 2008. From 2002 to 2006, he was with the Department of Electrical Engineering, University of Novi Sad as a Research Assistant, and from 2006 to 2009 with Liverpool John Moores University as a Research Associate.

From 2009 till 2013, he was with ABB Corporate Research Centre, Switzerland, as a Principal Scientist working on the power electronics projects spanning the range from low- voltage/power SMPS in the below kilowatt range to medium voltage high-power converters in the megawatt range. During 2010-2011, he was a member of a project team responsible for the development of the worlds first power electronic traction transformer (PETT) successfully commissioned on the locomotive. From 2013 till 2014, he was with ABB Medium Voltage Drives, Turgi, Switzerland, as R& D Platform Manager, responsible for ABBs largest IGCT based medium voltage drive - ACS6000. He is currently with École Polytechnique Fédérale de Lausanne (EPFL), Lausanne, Switzerland, as Assistant Professor and Director of the Power Electronics Laboratory. His current research interests include the areas of design and control of advanced high-power electronics systems and high performance drives.

Prof. Dujic has authored or coauthored more than 100 scientific publications and has filed eleven patents. He is an Associate Editor for IEEE Transactions on Industrial Electronics, IEEE Transaction on Power Electronics and IET Electric Power Applications. He has received the First Prize Paper Award by the Electric Machines Committee of the IEEE Industrial Electronics Society at IECON-2007. In 2014 he has received the Isao Takahashi Power Electronics Award for outstanding achievement in power electronics.